ACS APPLIED MATERIALS & INTERFACES

Research Article

www.acsami.org

$CoMoO_4$ Nanoparticles Anchored on Reduced Graphene Oxide Nanocomposites as Anodes for Long-Life Lithium-Ion Batteries

Jianyu Yao,[†,‡] Yongji Gong,[§] Shubin Yang,*[,†,∥] Peng Xiao,[⊥] Yunhuai Zhang,*[,‡] Kunttal Keyshar,[†] Gonglan Ye,[†] Sehmus Ozden,[†] Robert Vajtai,[†] and Pulickel M. Ajayan*[,†,§]

[†]Department of Materials Science and NanoEngineering and [§]Department of Chemistry, Rice University, 6100 Main Street, Houston, Texas 77005, United States

[‡]College of Chemistry and Chemical Engineering and [⊥]College of Physics, Chongqing University, Chongqing 400044, P. R. China

[∥]School of Materials Science and Engineering, Beihang University, Beijing, P. R. China

Supporting Information

ABSTRACT: A self-assembled $CoMoO_4$ nanoparticles/reduced graphene oxide ($CoMoO_4$NP/rGO), was prepared by a hydrothermal method to grow 3−5 nm sized $CoMoO_4$ particles on reduced graphene oxide sheets and used as an anode material for lithium-ion batteries. The specific capacity of $CoMoO_4$NP/rGO anode can reach up to 920 mAh g^{-1} at a current rate of 74 mA g^{-1} in the voltage range between 3.0 and 0.001 V, which is close to the theoretical capacity of $CoMoO_4$ (980 mAh g^{-1}). The fabricated half cells also show good rate capability and impressive cycling stability with 8.7% capacity loss after 600 cycles under a high current density of 740 mA g^{-1}. The superior electrochemical performance of the synthesized $CoMoO_4$NP/rGO is attributed to the synergetic chemical coupling effects between the conductive graphene networks and the high lithium-ion storage capability of $CoMoO_4$ nanoparticles.

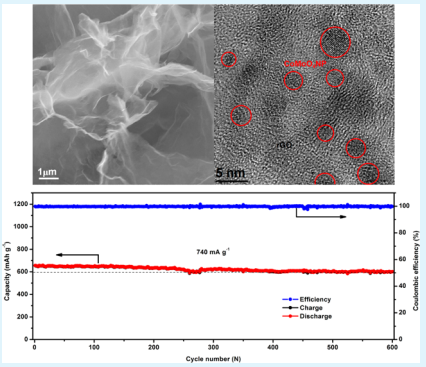

KEYWORDS: *$CoMoO_4$ nanoparticles, reduced graphene oxide, hydrothermal synthesis, lithium-ion batteries, anode materials*

1. INTRODUCTION

Lithium-ion batteries (LIBs) are considered the most prominent power sources for state-of-the-art mobile communication devices, portable electronic devices, and electrical/hybrid vehicles. Developing high specific energy, long cycle life, low-price, and environmentally friendly cathode/anode materials for LIBs are the key factors for practical applications.[1,2] Graphene, a two-dimensional (2D) carbon atom monolayer, has been commonly studied as anode material because of its large specific surface area (2630 m^2 g^{-1}), superior electrical conductivity, chemical stability, structural flexibility, as well as a high theoretical lithium storage capacity of 744 mAh g^{-1}.[3−9] To increase capacity, researchers have prepared many nanostructured transition-metal oxide/graphene composites: TiO_2/graphene,[10] Mn_3O_4/graphene,[11] FeO_x/graphene,[12−14] Co_3O_4/graphene,[15] NiO/graphene,[16] CuO/graphene,[17] MoO_2/graphene,[18] etc. Compared with their bare carbon materials, these composites exhibit considerably better cell stability, higher capacities, and better rate capability attributed to the synergetic chemical coupling effects between the conductive graphene networks and the high lithium-ion storage capability of transition-metal oxide. Besides, nanosized particles rather than their bulk materials are employed in the most cases due to the following reasons: (1) nanomaterials can significantly shorten the lithium diffusion path length compared to their bulk counterpart;[19] (2) the small-sized material is able to partially buffer the physical strains during the lithium insertion/extraction;[20] (3) the high surface area permits a higher contact area between electrolyte and electrode, thus improving the reaction kinetics.[14,21−23] Regardless of these advances, crack and pulverization of the nanomaterials and cell degradation are usually unavoidable. This mechanical degradation is explained by the restacking process of 2D graphene nanosheets with nanoparticles because of van der Waals forces and the weak interaction between graphene nanosheet and nanoparticles, resulting in loss of the advantages of a separated atomic layer state.[23,24]

Three-dimensional (3D) porous structure with large surface area, low mass density, and high electrical conductivity is an ideal scaffold to serve as a hybrid electrode.[25,26] In addition, 3D-graphene can potentially utilize the vertical dimension to increase the active material loading, enhance the interfacial kinetics and provide sufficient space to accommodate the stress relaxation.[27] Therefore, it is highly desirable to utilize 3D graphene frameworks in hybrid nanocomposites for long cycle life and stability in lithium-ion battery anodes compared to unstructured graphene. $CoMoO_4$ has been widely used in supercapacitors because of its excellent rate capability and cycling stability with 3D graphene network structure.[9,26,28−31] Although $CoMoO_4$ has a high theoretical capacity of 980 mAh

Received: September 3, 2014
Accepted: November 7, 2014
Published: November 7, 2014

g^{-1} used as LIB anodes, its low electronic conductivity, rapid capacity loss, and poor capacity retention have hampered its practical applications.[32] With the optimized particle size of $CoMoO_4$ and structuring with a graphene scaffold, these problems could potentially be solved, which would allow good electrolyte permeability and fast electron and ion transport.[33]

Herein, we report a facile hydrothermal method for synthesizing a hybrid material composed of $CoMoO_4$ nanoparticles grown on reduced graphene oxide and its application as an anode for lithium-ion batteries. Using the 3D graphene architecture as an excellent scaffold to host 3−5 nm $CoMoO_4$ particles is the key to improving its electrochemical performance. The multilevel porous structure and high surface area of the $CoMoO_4$NP/rGO nanocomposites improve conductivity and shorten lithium path length during the lithium insertion/extraction process. These advantages of this advanced structure lead to higher capacity and better cycling stability compared to pristine $CoMoO_4$ or rGO.

2. EXPERIMENTAL SECTION

2.1. Materials Synthesis. *Synthesis of GO and $CoMoO_4$ precursor.* Graphene oxide (GO) nanosheets were synthesized from a commercial graphite (SP-1 graphite, purchased from Bay Carbon Corporation) according to a modified Hummers method,[34] described elsewhere.[35,36] 4 mmol of $Co(NO_3)_2{\cdot}6H_2O$ and 4 mmol of H_2MoO_4 (molybdic acid) was dispersed in 45 mL distilled water under constant magnetic stirring, the solution became instantly pink. In order to increase the solubility of molybdic acid, 5 mL $NH_3{\cdot}H_2O$ (ammonium hydroxide) was added dropwise to the solution. With the addition of $NH_3{\cdot}H_2O$, a deposit settled in the bottom of the solution and then turned clear dark brown and it remained unchanged after 1 h of stirring. Finally, the mixture as $CoMoO_4$ precursor gives a clear dark brown solution with the Co:Mo mole ratio close to 1.

Synthesis of $CoMoO_4$NP/rGO. $CoMoO_4$ nanoparticles doped on reduced Graphene oxide (denoted as $CoMoO_4$NP/rGO) were synthesized by a simultaneous hydrothermal synthesis and assembly procedure. In a typical procedure, x mL (x = 1, 3, 6) $CoMoO_4$ precursor was mixed with 10 mL of GO (1 mg mL^{-1}) aqueous dispersion and sonicated for 1 h. The resulting mixture was then sealed in a Teflon-lined stainless steel autoclave (100 mL) and hydrothermally treated at 180 °C for 12 h. After cooling to room temperature, the product was washed thoroughly with deionized water and ethanol several times, and freeze-dried to preserve the 3D architectures formed during synthesis process. Finally, the $CoMoO_4$NP/rGO hybrids were obtained, the $CoMoO_4$ content were controlled to be 65, 74, and 88 wt %, respectively. As a reference, bare $CoMoO_4$ without GO and pure rGO were also prepared under the same experimental conditions.

2.2. Materials Characterization. The morphology, microstructure, and composition of the samples were systematically investigated by FE-SEM (JEOL 6500), TEM (JEOL 2010), XPS (PHI Quantera X-ray photoelectron spectrometer), XRD (Rigaku D/Max Ultima II Powder X-ray diffractometer), EDX (energy-dispersive X-ray spectroscopy, FEI Quanta 400 ESEM FEG) and TGA (thermogravimetric analysis, Q-600 Simultaneous TGA/DSC). Nitrogen adsorption isotherms and the Brunauer−Emmett−Teller (BET) surface area were measured at 77 K with a Quantachrome Autosorb-3B analyzer (USA).

2.3. Electrochemical Measurements. Electrochemical experiments were performed using CR2032 coin-type cells: the working electrodes were prepared by mixing our samples, carbon black (Super-P), and polyvinylidene fluoride (PVDF) at a weight ratio of 80:10:10 in n-methyl-2-pyrrolidone (NMP) solution. The obtained slurry was then pasted on pure copper foil (99.6%, Goodfellow), followed by drying them in a vacuum oven at 85 °C for 12 h. Pure lithium foil (Aldrich) was used as the counter electrode. The electrolyte, purchased from MTI Corporation, consists of 1 M $LiPF_6$ in a 1:1:1 mixture of ethylene carbonate (EC)/dimethyl carbonate (DMC)/diethyl carbonate (DEC). The cells were assembled in an argon-filled glovebox with the concentrations of moisture and oxygen below 0.1 ppm. CV curves were recorded on an Arbin BT-2000 battery station at a scanning rate of 0.1 mV s^{-1} at room temperature. The electrochemical performance measurements were carried out on a LAND CT2001A battery system tester at various current rates in the voltage range of 0.01−3.0 V. The impedance spectra were recorded on an Autolab workstation (PGSTAT302N) by applying a sine wave with amplitude of 5.0 mV over the frequency range from 100 kHz to 0.01 Hz.

3. RESULTS AND DISCUSSION

The preparation procedure of $CoMoO_4$NP/rGO nanocomposites is illustrated in Figure 1 (for details, see the Experimental Section). First, $Co(NO_3)_2{\cdot}6H_2O$ and H_2MoO_4 was dispersed in distilled water under constant magnetic stirring. Then an excessive amount of $NH_3{\cdot}H_2O$ was added in the solution to form the $[Co(NH_3)_6]MoO_4$ precursor. Finally, the precursor was dispersed in GO suspension. Under ultrasonication, Co^{3+} and Mo^{6+} ions were adsorbed onto the GO surface because of the functional groups (e.g., −OH, −COOH) and defects of GO surface.[33,37] The following reactions describe the stepwise formation of $[Co(NH_3)_6]MoO_4$ precursor and the subsequent hydrothermal treatment

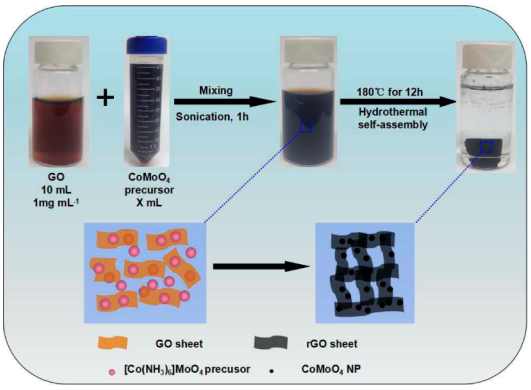

Figure 1. Photographs and schematic representation of the formation of $CoMoO_4$NP/rGO hybrid nanostructures. Purple and dark balls represent the $CoMoO_4$ precursor ($[Co(NH_3)_6]MoO_4$) and the $CoMoO_4$ nanoparticles, respectively.

$$H_2MoO_4 + 2NH_3{\cdot}H_2O \rightarrow (NH_4)_2MoO_4 + 2H_2O \quad (1)$$

$$Co(NO_3)_2{\cdot}6H_2O + 2NH_3{\cdot}H_2O \rightarrow Co(OH)_2 \downarrow + 2NH_4{\cdot}NO_3 + 6H_2O \quad (2)$$

$$Co(OH)_2 + 6NH_3{\cdot}H_2O \rightarrow [Co(NH_3)_6](OH)_2 + 6H_2O \quad (3)$$

$$[Co(NH_3)_6](OH)_2 + (NH_4)_2MoO_4 \rightarrow [Co(NH_3)_6]MoO_4 + 2NH_3{\cdot}H_2O \quad (4)$$

$$[Co(NH_3)_6]MoO_4 \rightarrow CoMoO_4 + 2NH_3\uparrow \quad (5)$$

Stirring and ultrasonication process was applied to ensure that the resulting precipitates were completely wrapped within GO sheets. In the subsequent hydrothermal treatment, $CoMoO_4$ nanoparticles were formed and embedded in graphene sheets. After the hydrothermal process, the nanoparticles have strong interactions or covalent bonds with graphene, and at the same

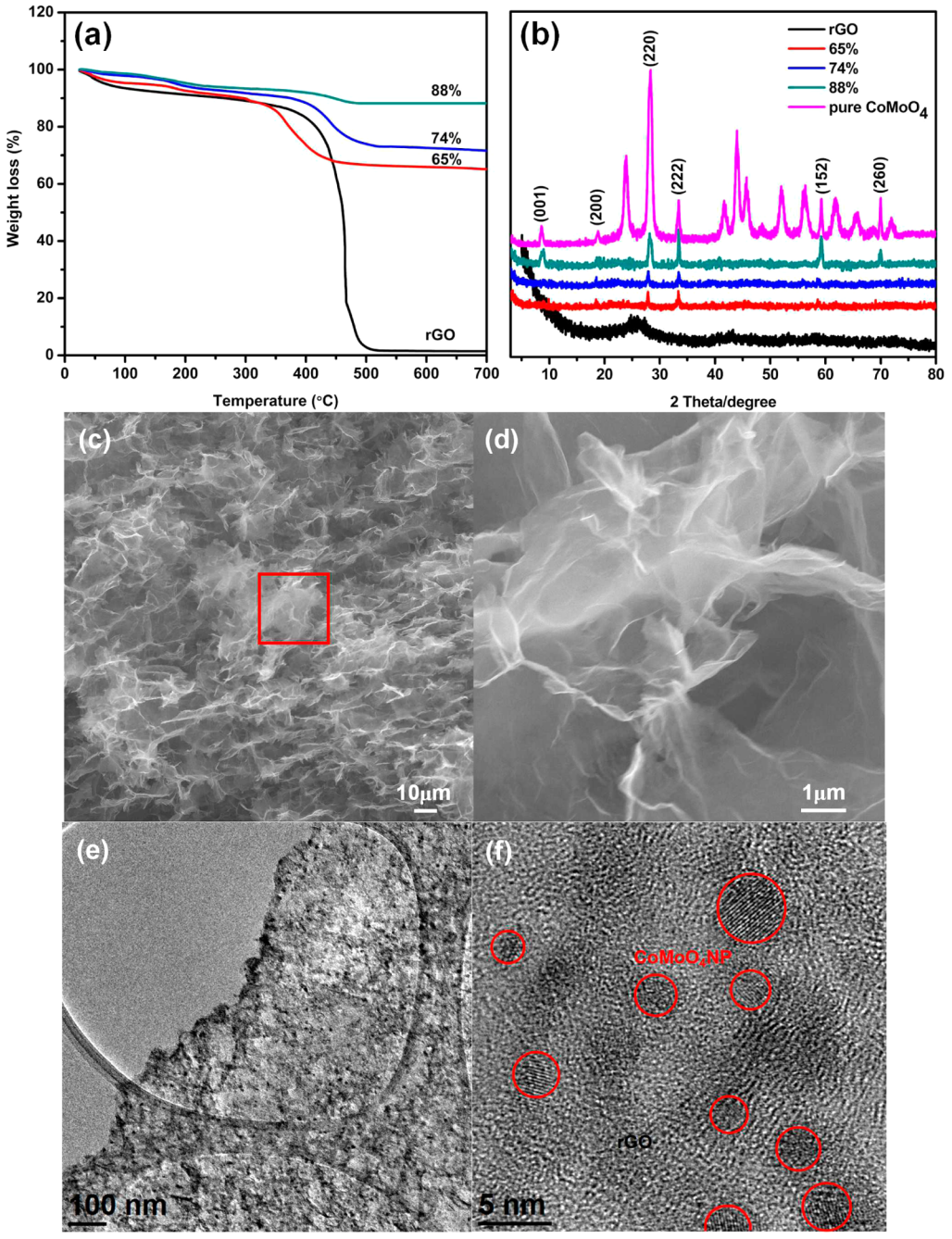

Figure 2. Thermogravimetric analysis (TGA) of $CoMoO_4$NP/rGO with different (a) $CoMoO_4$ contents and (b) XRD patterns. (c–f) Characterization of the morphology and elemental analysis of $CoMoO_4$NP/rGO (74%) nanocomposite. (c, d) Typical SEM images of the nanocomposite with different magnifications, revealing that the nanoparticles changed the structure of the graphene sheets. (e, f) TEM images of the nanocomposite, showing that the $CoMoO_4$ nanoparticles are confined in the matrix of the graphene nanosheets.

time GO is reduced to rGO without postsynthetic annealing or calcination.[38,39] Notably, the weight fractions of $CoMoO_4$ in the as-prepared 3D architectures were facilely controlled by adjusting the ratios between $CoMoO_4$ and rGO. In this text, all the contents of $CoMoO_4$ were calculated on the basis of weight fraction (wt %). The $CoMoO_4$ residues after oxidation in air in thermogravimetric analysis (TGA) are 65, 74, and 88% for the $CoMoO_4$NP/rGO nanocomposites synthesized with 1, 3, and 6 mL $CoMoO_4$ precursor mixed with 10 mL of GO suspension, respectively (Figure 2a). The TGA were carried out from 30 to 700 °C with a heating rate of 10 °C min^{-1} in air. Figure 2b displays the XRD patterns of rGO, $CoMoO_4$NP/rGO with different $CoMoO_4$ contents and pure $CoMoO_4$. At 26°, there is a wide diffraction peak, which can be attributed to the (002) planes of rGO. In the composite samples this peak is invisible, indicating that rGO flakes are well-separated by numerous $CoMoO_4$ nanoparticles. The orther XRD Peaks at 8.9, 18.7, 28, 34, 59, and 69.5° are attributed to the diffractions of (001), (200), (220), (222), (152), and (260) faces of the monoclinic $CoMoO_4$ (JCPDS NO: 21–0868).[26] An interesting phenomenon is that their intensities become stronger with increasing the content of $CoMoO_4$ in the hybrids.

Scanning electron microscopy (SEM) reveals the typical structure of the $CoMoO_4$NP/rGO (74%) (Figure 2c, d). The

dx.doi.org/10.1021/am505983m | ACS Appl. Mater. Interfaces 2014, 6, 20414–20422

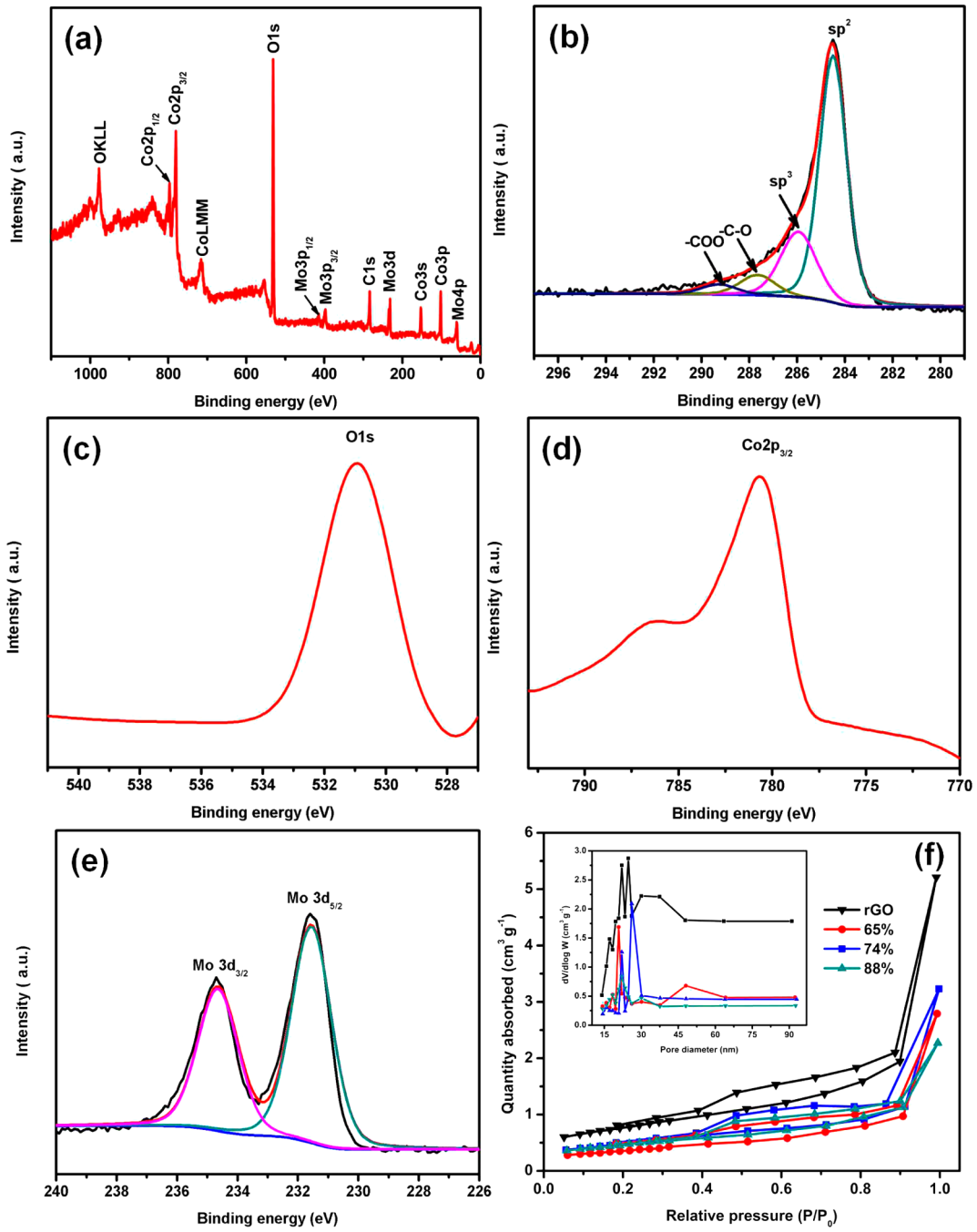

Figure 3. XPS survey spectrum of $CoMoO_4$ NP@rGO (74%): (a) full XPS survey spectrum, (b) C 1s core-level XPS, (c) O 1s core-level XPS, (d) Co 2p core-level XPS, and (e) Mo 3d core-level XPS; f) N_2 adsorption−desorption isotherms of rGO, and $CoMoO_4$NP/rGO with different $CoMoO_4$ contents. The inset in f is the corresponding pore-size distribution curves.

porous structure with atomically thin sheets indicates that the scaffold is built of stacked graphene sheets, the nanoparticles are not readily observable with the resolution of the SEM. In the low-magnification TEM, uniformly distributed dark contrast dots are easily observed on the graphene flakes (Figure 2e). A high-magnification TEM image in Figure 2f shows the crystal lattice of $CoMoO_4$. These tiny $CoMoO_4$ nanoparticles of 3−5 nm in size are densely anchored on the surface of graphene without aggregation, forming the hybrid $CoMoO_4$NP/rGO nanosheets. The fact that the nanoparticles do not form aggregates indicates that the graphene nanosheets play an essential role in achieving good dispersion. However, with increasing amount of the $CoMoO_4$ precursor during synthesis, the nanoparticles are stacked together, the 3D architecture is not maintained and the product is turned into micrometer scale powder after the hydrothermal reaction as shown in Figure S1. Thus, it is clear that the abundant functional groups and inherent flexibility of graphene oxide sheets are crucial for constructing the 3D hybrid architectures.

X-ray photoelectron spectroscopy (XPS) reveals that the $CoMoO_4$NP/rGO nanocomposites contain C, O, Co, and Mo as the main elements (Figure 3). The high-resolution C1 XPS spectrum signifies a number of functional groups on graphene sheets, such as hydroxyl (C−OH) and carboxyl (−COOH)

dx.doi.org/10.1021/am505983m | ACS Appl. Mater. Interfaces 2014, 6, 20414−20422

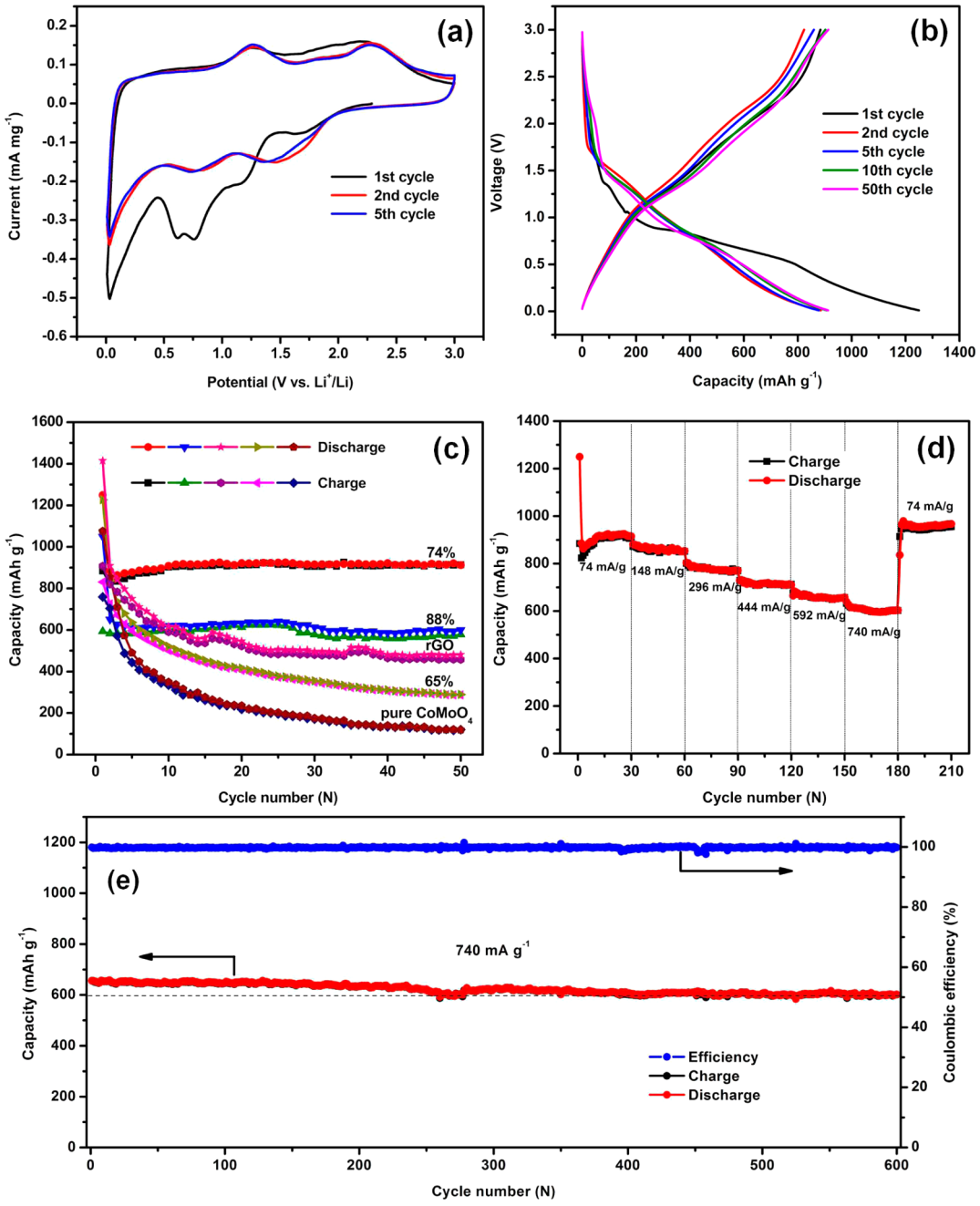

Figure 4. Electrochemical performances of $CoMoO_4$NP/rGO nanocomposites and pure $CoMoO_4$. (a) Cyclic voltammetry profiles of the 1st, 2nd, and 5th cycle for $CoMoO_4$NP/rGO (74%) nanocomposites in the voltage range from 0.01 to 3.0 V at a scanning rate of 0.1 mV s^{-1}; Li metal was used as the counter electrode. (b) Galvanostatic charge−discharge curves cycled at the 1st, 2nd, 5th, 10th, and 50th cycle of $CoMoO_4$NP/rGO (74%) between 3.0 and 0.01 V at a current density of 74 mA g^{-1}. (c) Cycling performances of $CoMoO_4$NP/rGO (65%), (74%), (88%), and pure $CoMoO_4$. (d) Rate capability of the $CoMoO_4$NP/rGO (74%) nanocomposite at the current densities between 74 and 740 mA g^{-1}. (e) Subsequent cycling test of the $CoMoO_4$NP/rGO (74%) at 740 mA g^{-1} for 600 cycles.

groups in Figure 3a, which might form the covalent chemical bonding, hydrogen bonding, or van der Waal's interaction with $CoMoO_4$ and enable direct growth of $CoMoO_4$ on the graphene sheets. The Co $2p_{3/2}$ core-level spectrum of $CoMoO_4$ is centered at 780.5 eV (Figure 3c), which belongs to Co^{2+}.[9,40,41] In the Mo 3d XPS region (Figure 3d), two peaks at 232.36 and 235.47 eV are observed. The binding energy and the splitting width (Mo 3d = 3.12 eV) are in good agreement with those reported for Mo^{6+}.[42,43] In addition, element analysis by XPS reveals that the atomic ratio of Co and Mo is 1:1.03, which is close to the stoichiometry of $CoMoO_4$. To gain further insight into the distribution of $CoMoO_4$NP/rGO nanocomposites, we performed energy-dispersive X-ray spectroscopy (EDX) elemental mapping (see Figure S2 in the Supporting Information). A typical EDX spectrum from the $CoMoO_4$NP/rGO (74%) nanocomposite suggests that the hybrid is composed of C, O, Co, and Mo elements. Figure S2 in the Supporting Information demonstrates the C, O, Co, and Mo elemental mapping of the $CoMoO_4$NP/rGO hybrid, showing that C, O, Co, and Mo are homogeneously distributed among the whole hybrid samples.

N_2 adsorption−desorption analysis was measured to study the pore structure and the specific surface area of the sample. N_2 adsorption−desorption isotherms and pore size distribution curves are shown in Figure 3f. The isotherms can be classified as type IV, revealing the mesoporous structure of the $CoMoO_4$NP/rGO nanocomposites. From the adsorption branch of the isotherm, the specific surface area of rGO, $CoMoO_4$NP/rGO (65%), (74%), and (88%) are 496, 372, 361, and 335 m^2 g^{-1} respectively, which are calculated by the Brunauer−Emmett−Teller (BET) method. The nanocomposite has a stacked structure of curved graphene nanosheets, and numerous $CoMoO_4$ nanoparticles are anchored on two sides of each graphene flake, consequently, the graphene sheets cannot really make two-directional bending,[3−9] resulting in the nanocomposite has abundant channels that are conducive to the insertion/extraction of lithium ions and the flow of electrolyte.[44] The pore size distributions (inset in Figure 3f) indicate that the $CoMoO_4$NP/rGO nanocomposites exhibit wide pore size distributions from 2 to 90 nm, further confirming the existence of mesopores and macropores. With a large surface area, conductive rGO, and a small size of $CoMoO_4$ active nanoparticles, such a nanocomposite is beneficial for lithium storage applications that require a sufficient interface for electrolyte access, low contact and charge-transfer impedance, and a short transport length for both lithium ions and electrons. Therefore, superior lithium storage properties could be expected for the as-prepared $CoMoO_4$NP/rGO nanocomposites.

Static and dynamic lithium storage processes in $CoMoO_4$NP/rGO nanocomposites were investigated by cyclic voltammetry (CV) and galvanostatic charge/discharge cycling. Figure 4a and Figure S3 in the Supporting Information exhibit the first, second, and fifth cycle for $CoMoO_4$NP/rGO (74%), pure $CoMoO_4$ and rGO at a scan rate of 0.1 mV s^{-1} in the voltage window of 0.01−3 V vs Li^+/Li. Several reduction and oxidation peaks can be clearly observed in the CV curves, implying that the sample has a multiple reaction mechanism, which could be characterized by the following equations[32,45]

$$CoMoO_4 + 8Li \rightarrow Co + Mo + 4Li_2O \quad (6)$$

$$Co + Li_2O \leftrightarrow CoO + 2Li \quad (7)$$

$$Mo + 3Li_2O \leftrightarrow MoO_3 + 6Li \quad (8)$$

$$C(\text{graphene}) + xLi + xe^- \leftrightarrow Li_xC \quad (9)$$

Five reduction peaks can be found in the cathodic polarization process of the first cycle (Figure 4a). The broad peak centered at 1.7 and 1.2 V should be attributed to the crystal structure destruct into amorphous and the reduction of Mo^{6+} to Mo^{4+},[46] the intense peak located at 0.74 V could be assigned to the further reduction of Co^{2+} and Mo^{4+} to metallic Co and Mo (eq 6), whereas the minor peak at 0.6 V can be ascribed to the irreversible decomposition of the solvent in the electrolyte to form the solid-electrolyte interface (SEI).[32,47] The fifth cathodic peak located at 0.01 V is attributed to the insertion of lithium in grephene nanosheets (eq 9).[45] Three obvious anodic peaks located at 0.13, 1.27, and 2.29 V were observed in the first anodic scan. The 0.13 V anodic peak corresponds to lithium extraction from graphene nanosheet (eq 9); the other two peaks at 1.27 and 2.29 V can be assigned to the oxidation of Co and Mo into CoO and MoO_3, which is fully reversible, according to the reaction of eqs 7 and 8. Compared with the first cathodic scan, there are two new cathodic peaks at 1.33 and 0.70 V, which can be ascribed to the electrochemical reduction of CoO and MoO_3 into Co and Mo (eqs 7 and 8).[18,32] Figure S3a in the Supporting Information shows the CV curves of pure $CoMoO_4$. Similar to those of $CoMoO_4$NP/rGO nanocomposites, the second cycle has sharp two cathodic/anodic peaks at about 1.33/1.27 V and 0.70/2.29 V. Nevertheless, both the peak intensity and integral areas decrease significantly during the subsequent cycles, indicating severe capacity fading. Remarkably, compared to pure $CoMoO_4$, the $CoMoO_4$NP/rGO (74%) CV curves are mostly overlapped from the second cycle onward, which indicates good reversibility of the electrochemical reactions.

Figure 4b presents the charge/discharge profiles of the $CoMoO_4$NP/rGO (74%) nanocomposite in the first, second, fifth, 10th, and 50th cycles at a current density of 74 mA g^{-1}. The discharge and charge capacities in the first cycle were 1250 and 880 mAh g^{-1}, respectively, with a first cycle capacity loss of 30%. High initial capacity loss is commonly observed for oxide anode materials.[46] However, the discharge capacities of the $CoMoO_4$NP/rGO nanocomposites are very close to the theoretical value ($C_{\text{theoretical}} = C_{\text{CoMoO4}} \times$ mass percentage of + $C_{\text{graphene}} \times$ mass percentage of graphite = 980 × 74% + 744 × 26% = 918 mAh g^{-1}).[32] The initial irreversible capacity results from the SEI formed in the first discharge process as well as the electrolyte decomposition at a low potential region around 0.5 V for the first cycle, as shown in Figure 4b.[32] Hereafter, the extra capacity could arise from reversible reactions of lithium with the active surface groups including dangling C−H and C-OOH bonds on the surface of rGO.[48,49] The improved performance may be attributed to synergistic interactions between the rGO sheets and $CoMoO_4$ nanoparticles. RGO may work as mechanical buffer that alleviates the volume change of the nanoparticles during charge and discharge.[50−52] Furthermore, the $CoMoO_4$ nanoparticles act as a spacer that prevents the rGO sheets from agglomeration.[52] To find out which electrode among the three different ratios has the highest specific capacity and best cycling performance, we tested 50 discharge/charge cycles as shown in Figure 4c. The cycling performance of the $CoMoO_4$NP/rGO (74%) was superior to that of pure $CoMoO_4$, rGO, $CoMoO_4$NP/rGO (65%) and (88%). The reversible capacity of the $CoMoO_4$NP/rGO (74%) gradually increases in the first 10 cycles and is stabilized at a high reversible capacity of 920 mAh g^{-1} after 50 cycles, and the Coulombic efficiency remains ∼ 100% upon cycling. The extraordinary performance of $CoMoO_4$NP/rGO (74%) mainly relies on its specific structure: on the one hand, 74% $CoMoO_4$NP in rGO has higher theoretical capacity than that of 65% $CoMoO_4$NP in rGO; on the other hand, more $CoMoO_4$ content, like 88% $CoMoO_4$NP in rGO (see Figure S1 in the Supporting Information), 3D structure of rGO would be broken, blocking the path of lithium insertion/extraction.

In addition, the $CoMoO_4$NP/rGO (74%) nanocomposite exhibits excellent rate capability. The rate performance was evaluated in the cell we used for the above-mentioned 50 cycles, as shown in Figure 4d; each rate was tested for 30 cycles. From Figure 4d, it can be seen that the capacity decreases from 920, 850, 770, 710 to 660 mAh g^{-1} with increasing current density ranging from 74, 150, 300, 440, 590 to 740 mA g^{-1}. Specific capacity retention of 64% is capable even with a ten times increase at current density from 74 to 740 mA g^{-1}. Interestingly, the $CoMoO_4$NP/rGO (74%) anode releases a higher reversible capacity (970 mAh g^{-1}) after the 210th cycle than its initial one. It can be detected that, in spite of high

current densities applied, the increasing slope (capacity versus cycle) in rate capability is approximately comparable to that in cycling performance conducted at the same 74 mA g^{-1} (Figure 4c), demonstrating a magnificent high rate performance. Figure 4e shows long-term cycling performance and the corresponding Coulombic efficiency of the nanocomposites at 740 mA g^{-1}. The $CoMoO_4$NP/rGO anode demonstrated excellent cycling stability above 600 mAh g^{-1} with 8.7% capacity loss and a Coulombic efficiency close to 100% over 600 cycles. Compared with other reported binary metal oxide/graphene composites, such as $CoFe_2O_4$/graphene,[53] $NiFe_2O_4$/graphene and $ZnFe_2O_4$/graphene,[54−56] etc., the $CoMoO_4$NP/rGO anode shows higher rate capability and longer cyclability. That is mainly attributed to $CoMoO_4$ have large cell parameters (a = 9.67, b = 8.85, c = 7.76 Å, p = 113°49′).[31−33,57] And it can keep the 3D architecture of rGO after mixing. The superior electrochemical performance of $CoMoO_4$NP/rGO anode can also be due to the synergistic effect between CoO and MoO_3 during cycling.[32]

To illustrate the lithium storage mechanisms and the structural evolution of $CoMoO_4$NP/rGO during the lithium insertion/extraction process, an ex situ XRD analysis has been carried out (see Figure S4 in the Supporting Information). Before cycle, the (222) peak of $CoMoO_4$ at 34° is very easy to observed. After the first discharge proceess, there is a very sharp peak around 38° belong to Li_2O, and it still turn up in the subsequent cycles. However, no obvious peaks of metallic Co, Mo, and Li_xC are visible in the patterns after the first extraction of lithium, although they can be detected through MDI Jade 9.0. That is probably due to their ultrafine size and poor crystallinity, or they are overlapped by the strong peaks of Cu current collector.[23,58] The existence of metallic Co and Mo further confirms the first lithiation mechanism of eq 6. Some peaks of CoO and MoO_3 at the eighth charge XRD are very difficult to observed. But they turned sharper after 600 cycles, especially around 38 and 65°. There is another new peak near by 79°, that is belong to Li_2F. The appearance of Li_2F is one reason for the capacity decrease.

To further understand why the $CoMoO_4$NP/rGO electrode exhibits such a superior electrochemical performance compared to the $CoMoO_4$ electrode, we performed ac impedance measurements after 50 cycles, as shown in Figure 5. The inclined line corresponds to the lithium-diffusion process within the bulk of the electrode material. The kinetic differences of $CoMoO_4$NP/rGO and pure $CoMoO_4$ electrodes were further investigated by modified Randles equivalent circuit (see the Supporting Information, Figure S5).[24] The fitted impedance parameters are listed in Table S1 in the Supporting Information. It can be seen that the SEI film resistance R_f and charge-transfer resistance R_{ct} of the $CoMoO_4$NP/rGO (74%) electrode are 4.0 and 132.8 Ω, which are significantly lower than those of pure $CoMoO_4$ (13.7 and 321.0 Ω). This fact confirms that the incorporation of graphene can preserve the high conductivity of the $CoMoO_4$NP/rGO composite electrode and greatly enhance rapid electron transport during the electrochemical lithium insertion/extraction reaction, resulting in significant improvement in the electrochemical performances. The structural stability of $CoMoO_4$NP/rGO nanocomposites was also investigated with SEM observation for tested cells. The electrodes were taken out from the coin cells after 1 cycle and 600 cycles and washed using a dimethyl carbonate solution. As shown in Figure S6a, b in the Supporting Information, no obvious changes in the morphology are observed, and the SEI films of the electrode are dense and slick, demonstrating the structure integrity of the composite upon electrochemical cycling. The structural stability of the composite can be ascribed to the directly grown structure that tightly connects the graphene film with $CoMoO_4$, preventing the detachment and agglomeration of $CoMoO_4$ nanoparticles during cycling, which contributes to the excellent cyclic stability.

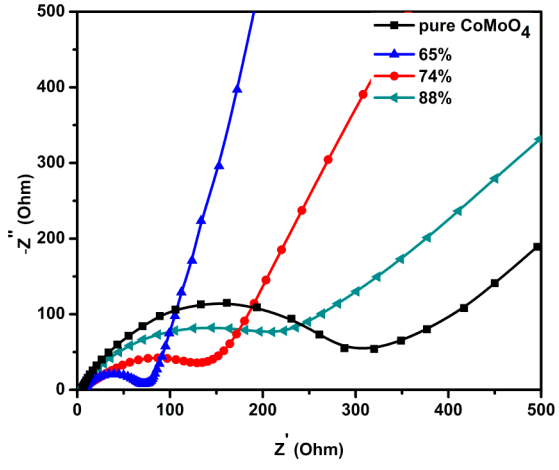

Figure 5. Nyquist plots of pure $CoMoO_4$ and $CoMoO_4$NP/rGO with different contents of $CoMoO_4$ obtained by applying a sine wave with amplitude of 5.0 mV over the frequency range 100 kHz to 0.01 Hz.

4. CONCLUSIONS

In summary, we have fabricated a structure of ultrathin $CoMoO_4$NP/rGO hybrid nanosheets through a facile hydrothermal method. The best performance was obtained on the composite with ∼26 wt % of rGO and 74% $CoMoO_4$. The $CoMoO_4$NP/rGO (74%) nanocomposites behave as high-performance anode materials with a specific capacity of 920 mAh g^{-1} at 74 mA g^{-1} specific current rate and 660 mAh g^{-1} at 740 mA g^{-1} rate. Especially, the $CoMoO_4$NP/rGO nanocomposites showed excellent cycling stability, only 8.7% capacity loss after 600 cycles under a high current density of 740 mA g^{-1}. The 3−5 nm $CoMoO_4$ nanoparticles hosted by the 3D graphene architectures can effectively shorten lithium diffusion paths, improve conductivity, as well as buffer the physical strains during the lithium-ion insertion/extraction. From these results, it can be concluded that $CoMoO_4$NP/rGO nanocomposites is very promising as a potential anode material for LIBs.

■ ASSOCIATED CONTENT

Supporting Information

Additional SEM, XPS, XRD, and mapping figures for $CoMoO_4$NP/rGO and rGO. This material is available free of charge via the Internet at http://pubs.acs.org.

■ AUTHOR INFORMATION

Corresponding Authors

*E-mail: yangshubin@buaa.edu.cn. Tel: +1-7133485904. Fax: +1-7133485423.
*E-mail: xp2031@163.com
*E-mail: ajayan@rice.edu..

Notes

The authors declare no competing financial interest.

■ ACKNOWLEDGMENTS

This work was financially supported by U.S. Army Research Office through the MURI grant (W911NF-11-1-0362) entitled, "Atomic Layers of Nitrides, Oxides, and Sulfides". P. M. A. also acknowledges funding sponsorship from the U.S. Air Force Office of Scientific Research for the MURI grant (FA9550-12-1-0035) entitled, "Synthesis and Characterization of 3-D Carbon Nanotube Solid Networks". Y. J.Y. gratefully acknowledges the financial support from the China Scholarship Council (CSC) during her visit to Rice University.

■ REFERENCES

(1) Pan, D. Y.; Wang, S.; Zhao, B.; Wu, M. H.; Zhang, H.; Wang, Y.; Jiao, Z. Li Storage Properties of Disordered Graphene Nanosheets. *Chem. Mater.* **2009**, *21*, 3136−3142.

(2) Yao, Y.; McDowell, M. T.; Ryu, I.; Wu, H.; Liu, N.; Hu, L. B.; Nix, W. D.; Cui, Y. Interconnected Silicon Hollow Nanospheres for Lithium-Ion Battery Anodes with Long Cycle Life. *Nano Lett.* **2011**, *11*, 2949−2954.

(3) Geim, A. K. Graphene: Status and Prospects. *Science* **2009**, *324*, 1530−1534.

(4) Peng, C. X.; Chen, B. D.; Qin, Y.; Yang, S. H.; Li, C. Z.; Zuo, Y. H.; Liu, S. Y.; Yang, J. H. Facile Ultrasonic Synthesis of CoO Quantum Dot/Graphene Nanosheet Composites with High Lithium Storage Capacity. *ACS Nano* **2012**, *6*, 1074−1081.

(5) Bolotin, K. I.; Sikes, K. J.; Jiang, Z.; Klima, M.; Fudenberg, G.; Hone, J.; Kim, P.; Stormer, H. L. Ultrahigh Electron Mobility in Suspended Graphene. *Solid State Commun.* **2008**, *146*, 351−355.

(6) Pumera, M. Graphene-based Nanomaterials and Their Electrochemistry. *Chem. Soc. Rev.* **2010**, *39*, 4146−4157.

(7) Wu, Z. S.; Zhou, G. M.; Yin, L. C.; Ren, W. C.; Li, F.; Cheng, H. M. Graphene/metal oxide Composite Electrode Materials for Energy Storage. *Nano Energy* **2012**, *1*, 107−131.

(8) Zhu, Y.; Murali, S.; Cai, W.; Li, X.; Suk, J. W.; Potts, J. R.; Ruoff, R. S. Graphene and Graphene Oxide: Synthesis, Properties, and Applications. *Adv. Mater.* **2010**, *22*, 3906−3924.

(9) Xia, X. F.; Lei, W.; Hao, Q. L.; Wang, W. J.; Wang, X. One-step Synthesis of CoMoO4/graphene Composites with Enhanced Electrochemical Properties for Supercapacitors. *Electrochim. Acta* **2013**, *99*, 253−261.

(10) Wang, D. H.; Choi, D. W.; Li, J.; Yang, Z. G.; Nie, Z. M.; Kou, R.; Hu, D. H.; Wang, C. M.; Saraf, L. V.; Zhang, J. G.; Aksay, I. A.; Liu, J. Self-Assembled TiO_2-Graphene Hybrid Nanostructures for Enhanced Li-Ion Insertion. *ACS Nano* **2009**, *3*, 907−914.

(11) Wang, H. L.; Cui, L. F.; Yang, Y.; Casalongue, H. S.; Robinson, J. T.; Liang, Y. Y.; Cui, Y.; Dai, H. J. Mn_3O_4-Graphene Hybrid as a High-Capacity Anode Material for Lithium Ion Batteries. *J. Am. Chem. Soc.* **2010**, *132*, 13978−13980.

(12) Su, J.; Cao, M. H.; Ren, L.; Hu, C. W. Fe_3O_4-Graphene Nanocomposites with Improved Lithium Storage and Magnetism Properties. *J. Phys. Chem. C* **2011**, *115*, 14469−14477.

(13) Lian, P. C.; Zhu, X. F.; Xiang, H. F.; Li, Z.; Yang, W. S.; Wang, H. H. Enhanced Cycling Performance of Fe_3O_4-graphene Nanocomposite as an Anode Material for Lithium-ion Batteries. *Electrochim. Acta* **2010**, *56*, 834−840.

(14) Zhou, G. M.; Wang, D. W.; Li, F.; Zhang, L. L.; Li, N.; Wu, Z. S.; Wen, L.; Lu, G. Q.; Cheng, H. M. Graphene-Wrapped Fe_3O_4 Anode Material with Improved Reversible Capacity and Cyclic Stability for Lithium Ion Batteries. *Chem. Mater.* **2010**, *22*, 5306−5313.

(15) Li, B. J.; Cao, H. Q.; Shao, J.; Li, G. Q.; Qu, M. Z.; Yin, G. Co_3O_4@graphene Composites as Anode Materials for High-Performance Lithium Ion Batteries. *Inorg. Chem.* **2011**, *50*, 1628−1632.

(16) Zou, Y. Q.; Wang, Y. NiO Nanosheets Grown on Graphene Nanosheets as Superior Anode Materials for Li-ion Batteries. *Nanoscale* **2011**, *3*, 2615−2620.

(17) Wang, B.; Wu, X. L.; Shu, C. Y.; Guo, Y. G.; Wang, C. R. Synthesis of CuO/graphene Nanocomposite as a High-performance Anode Material for Lithium-ion Batteries. *J. Mater. Chem.* **2010**, *20*, 10661−10664.

(18) Sun, Y. M.; Hu, X. H.; Luo, W.; Huang, Y. H. Self-Assembled Hierarchical MoO_2/Graphene Nanoarchitectures and Their Application as a High-Performance Anode Material for Lithium-Ion Batteries. *ACS Nano* **2011**, *5*, 7100−7107.

(19) Wang, Y.; Zhang, H. J.; Lu, L.; Stubbs, L. P.; Wong, C. C.; Lin, J. Y. Designed Functional Systems from Peapod-like Co@Carbon to Co_3O_4@Carbon Nanocomposites. *ACS Nano* **2010**, *4*, 4753−4761.

(20) Guo, Y. G.; Hu, J. S.; Wan, L. J. Nanostructured Materials for Electrochemical Energy Conversion and Storage Devices. *Adv. Mater.* **2008**, *20*, 2878−2887.

(21) Bruce, P. G.; Scrosati, B.; Tarascon, J.-M. Nanomaterials for Rechargeable Lithium Batteries. *Angew. Chem., Int. Ed.* **2008**, *47*, 2930−2946.

(22) Chen, Y.; Song, B. H.; Li, M.; Lu, L.; Xue, J. M. Fe_3O_4 Nanoparticles Embedded in Uniform Mesoporous Carbon Spheres for Superior High-Rate Battery Applications. *Adv. Funct. Mater.* **2014**, *24*, 319−326.

(23) Sun, Y. M.; Hu, X. L.; Luo, W.; Huang, Y. H. Ultrathin CoO/Graphene Hybrid Nanosheets: A Highly Stable Anode Material for Lithium-Ion Batteries. *J. Phys. Chem. C* **2012**, *116*, 20794−20799.

(24) Gong, Y. J.; Yang, S. B.; Zhan, L.; Ma, L. L.; Vajtai, R.; Ajayan, P. M. A Bottom-Up Approach to Build 3D Architectures from Nanosheets for Superior Lithium Storage. *Adv. Funct. Mater.* **2014**, *24*, 125−130.

(25) Chen, W. F.; Li, S.; Chen, C. H.; Yan, L. F. Self-Assembly and Embedding of Nanoparticles by In Situ Reduced Graphene for Preparation of a 3D Graphene/Nanoparticle Aerogel. *Adv. Mater.* **2011**, *23*, 5679−5683.

(26) Yu, X. Z.; Lu, B. G.; Xu, Z. Super Long-Life Supercapacitors Based on the Construction of Nanohoneycomb-Like Strongly Coupled $CoMoO_4$-3D Graphene Hybrid Electrodes. *Adv. Mater.* **2014**, *26*, 1044−1051.

(27) Liu, B. R.; Soares, P.; Checkles, C.; Zhao, Y.; Yu, G. H. Three-Dimensional Hierarchical Ternary Nanostructures for High-Performance Li-Ion Battery Anodes. *Nano Lett.* **2013**, *13*, 3414−3419.

(28) Smith, G. W.; Ibers, J. A. The Crystal Structure of Cobalt Molybdate $CoMoO_4$. *Acta Crystallogr.* **1965**, *19*, 269−275.

(29) Liu, M. C.; Kong, L. B.; Ma, X. J.; Lu, C.; Li, X. M.; Luo, Y. C.; Kang, L. Hydrothermal Process for the Fabrication of CoMoO 4 • 0.9 H_2O Nanorods with Excellent Electrochemical Behavior. *New J. Chem.* **2012**, *36*, 1713−1716.

(30) Mai, L. Q.; Yang, F.; Zhao, Y. L.; Xu, X.; Xu, L.; Luo, Y. Z. Hierarchical $MnMoO_4$/$CoMoO_4$ Heterostructured Nanowires with Enhanced Supercapacitor Performance. *Nat. Commun.* **2011**, *2*, 381−385.

(31) Liu, M. C.; Kong, L. B.; Lu, C.; Ma, X. J.; Li, X. M.; Luo, Y. C.; Kang, L. Design and Synthesis of $CoMoO_4$-$NiMoO_4$•xH_2O Bundles with Improved Electrochemical Properties for Supercapacitors. *J. Mater. Chem. A* **2013**, *1*, 1380−1387.

(32) Cherian, C. T.; Reddy, M. V.; Haur, S. C.; Chowdari, B. V. R. Interconnected Network of $CoMoO_4$ Submicrometer Particles as High Capacity Anode Material for Lithium Ion Batteries. *ACS Appl. Mater. Interfaces* **2013**, *5*, 918−923.

(33) Wu, Z. S.; Ren, W. C.; Wen, L.; Gao, L. B.; Zhao, J. P.; Chen, Z. P.; Zhou, G. M.; Li, F.; Cheng, H. M. Graphene Anchored with Co_3O_4 Nanoparticles as Anode of Lithium Ion Batteries with Enhanced Reversible Capacity and Cyclic Performance. *ACS Nano* **2010**, *4*, 3187−3194.

(34) Hummers, W. S.; Offeman, R. E. Preparation of Graphitic Oxide. *J. Am. Chem. Soc.* **1958**, *80*, 1339−1339.

(35) Liang, Y. Y.; Frisch, J.; Zhi, L. J.; Norouzi-Arasi, H.; Feng, X. L.; Rabe, J. P.; Koch, N.; Mullen, K. Transparent, Highly Conductive

Graphene Electrodes from Acetylene-assisted Thermolysis of Graphite Oxide Sheets and Nanographene Molecules. *Nanotechnology* **2009**, *20*, 434007.
(36) Yang, S. B.; Sun, Y.; Chen, L.; Hernandez, Y.; Feng, X. L.; Mullen, K. Porous Iron Oxide Ribbons Grown on Graphene for High-Performance Lithium Storage. *Sci. Rep.* **2012**, *2*, 427−433.
(37) Dreyer, D. R.; Park, S.; Bielawski, C. W.; Ruoff, R. S. The Chemistry of Graphene Oxide. *Chem. Soc. Rev.* **2010**, *39*, 228−240.
(38) Chang, H. X.; Wu, H. K. Graphene-based Nanocomposites: Preparation, Functionalization, and Energy and Environmental Applications. *Energy Environ. Sci.* **2013**, *6*, 3483−3507.
(39) Huang, X.; Qi, X. Y.; Boey, F.; Zhang, H. Graphene-based Composites. *Chem. Soc. Rev.* **2012**, *41*, 666−686.
(40) Wang, S. N.; Gao, Q. S.; Zhang, Y. H.; Gao, J.; Sun, X. H.; Tang, Y. Controllable Synthesis of Organic-Inorganic Hybrid MoO_x/Polyaniline Nanowires and Nanotubes. *Chem. -Eur. J.* **2011**, *17*, 1465−1472.
(41) Huang, X. L.; Chai, J.; Jiang, T.; Wei, Y. J.; Chen, G.; Liu, W. Q.; Han, D. X.; Niu, L.; Wang, L. M.; Zhang, X. B. Self-assembled Large-area $Co(OH)_2$ Nanosheets/ionic Liquid Modified Graphene Heterostructures Toward Enhanced Energy Storage. *J. Mater. Chem.* **2012**, *22*, 3404−3410.
(42) Ko, J. M.; Soundarajan, D.; Park, J. H.; Yang, S. D.; Kim, S. W.; Kim, K. M.; Yu, K. H. γ-Ray-induced Synthesis and Electrochemical Properties of a Mesoporous Layer-structured α-$Co(OH)_2$ for Supercapacitor Applications. *Curr. Appl. Phys.* **2012**, *12*, 341−345.
(43) Zheng, L.; Xu, Y.; Jin, D.; Xie, Y. Polyaniline-Intercalated Molybdenum Oxide Nanocomposites: Simultaneous Synthesis and their Enhanced Application for Supercapacitor. *Chemistry-An Asian J.* **2011**, *6*, 1505−1514.
(44) Lu, H. L.; Li, N. W.; Zheng, M. B.; Qiu, L.; Zhang, S. T.; Zheng, J. F.; Ji, G. B.; Cao, J. M. Microwave-assisted Synthesis of Graphene-SnO_2 Nanocomposite for Rechargeable Lithium-ion Batteries. *Mater. Lett.* **2014**, *115*, 125−128.
(45) Ji, L. W.; Lin, Z.; Alcoutlabi, M.; Zhang, X. W. Recent Developments in Nanostructured Anode Materials for Rechargeable Lithium-ion Batteries. *Energy Environ. Sci.* **2011**, *4*, 2682−2699.
(46) Hu, L.; Zhong, H.; Zheng, X. R.; Huang, Y. M.; Zhang, P.; Chen, Q. W. $CoMn_2O_4$ Spinel Hierarchical Microspheres Assembled with Porous Nanosheets as Stable Anodes for Lithium-ion Batteries. *Sci. Rep.* **2012**, *2*, 986.
(47) Zhu, X. J.; Zhu, Y. W.; Murali, S. T.; Stoller, M. D.; Ruoff, R. S. Nanostructured Reduced Graphene Oxide/Fe_2O_3 Composite As a High-Performance Anode Material for Lithium Ion Batteries. *ACS Nano* **2011**, *5*, 3332−3338.
(48) Ji, X. L.; Herle, P. S.; Rho, Y.; Nazar, L. F. Carbon/MoO_2 Composite Based on Porous Semi-Graphitized Nanorod Assemblies from In Situ Reaction of Tri-Block Polymers. *Chem. Mater.* **2007**, *19*, 374−383.
(49) Dahn, J. R.; Zheng, T.; Liu, Y.; Xue, J. S. Mechanisms for Lithium Insertion in Carbonaceous Materials. *Science* **1995**, *270*, 590−593.
(50) Allen, M. J.; Tung, V. C.; Kaner, R. B. Honeycomb Carbon: A Review of Graphene. *Chem. Rev.* **2010**, *110*, 132−145.
(51) Xu, Y.; Yi, R.; Yuan, B.; Wu, X. F.; Dunwell, M.; Lin, Q. L.; Fei, L.; Deng, S. G.; Andersen, P.; Wang, D. H.; Luo, H. M. High Capacity MoO_2/Graphite Oxide Composite Anode for Lithium-Ion Batteries. *J. Phys. Chem. Lett.* **2012**, *3*, 309−314.
(52) Yang, J.; Winter, M.; Besenhard, J. O. Small Particle Size Multiphase Li-alloy Anodes for Lithium-ion Batteries. *Solid State Ionics* **1996**, *90*, 281−287.
(53) Xia, H.; Zhu, D. D.; Fu, Y. S.; Wang, X. $CoFe_2O_4$-graphene Nanocomposite as a High-capacity Anode Material for Lithium-ion Batteries. *Electrochim. Acta* **2012**, *83*, 166−174.
(54) Fu, Y. S.; Wan, Y. H.; Xia, H.; Wang, X. Nickel Ferriteegraphene Heteroarchitectures: Toward High-performance Anode Materials for Lithium-ion Batteries. *J. Power Sources* **2012**, *213*, 338−342.
(55) Song, W. T.; Xie, J.; Liu, S. Y.; Cao, G. S.; Zhu, T. J.; Zhao, X. B. Self-assembly of a $ZnFe_2O_4$/graphene Hybrid and its Application as a High-performance Anode Material for Li-ion Batteries. *New J. Chem.* **2012**, *36*, 2236−2241.
(56) Xia, H.; Qian, Y. Y.; Fu, Y. S.; Wang, X. Graphene Anchored with $ZnFe_2O_4$ Nanoparticles as a High-capacity Anode Material for Lithium-ion Batteries. *Solid State Sci.* **2013**, *17*, 67−71.
(57) Xiao, W.; Chen, J. S.; Li, C. M.; Xu, R.; Lou, X. W. Synthesis, Characterization, and Lithium Storage Capability of $AMoO_4$ (A = Ni, Co) Nanorods. *Chem. Mater.* **2010**, *22*, 746−754.
(58) Sun, Y. M.; Hu, X. L.; Luo, W.; Shu, J.; Huang, Y. H. Self-assembly of Hybrid $Fe_2Mo_3O_8$-reduced Graphene Oxide Nanosheets with Enhanced Lithium Storage Properties. *J. Mater. Chem. A* **2013**, *1*, 4468−4474.